NATIONAL INSTITUTE FOR FUSION SCIENCE

On Stimulated Scattering of Laser Light in
Inertial Fusion Energy Targets

Lj. Nikolić, M.M. Škorić, S. Ishiguro and T. Sato

On Stimulated Scattering of Laser Light in Inertial Fusion Energy Targets

Lj. Nikolić[1], M. M. Škorić[2,3], S. Ishiguro[3], and T. Sato[4]

November 12, 2002

[1]The Graduate University for Advanced Studies, National Institute for Fusion Science, 322-6 Oroshi-cho, Toki-shi 509-5292, Japan

[2]Vinča Institute of Nuclear Sciences, POB 522, 11001 Belgrade, Yugoslavia

[3]Theory and Computer Simulation Center, National Institute for Fusion Science, 322-6 Oroshi-cho, Toki-shi 509-5292, Japan

[4]Earth Simulator Center, JAMSTEC, 3173-25 Showa-cho, Yokohama-shi 236-0001, Japan

Abstract

Propagation of a laser light through regions of an underdense plasma is an active research topic in laser fusion. In particular, a large effort has been invested in studies of stimulated Raman scattering (SRS) and stimulated Brillouin scattering (SBS) which can reflect laser energy and produce energetic particles to preheat a fusion energy target. Experiments, theory and simulations agree on a complex interplay between various laser-plasma instabilities. By particle-in-cell simulations of an underdense electron-plasma, we have found, apart from the standard SRS, a strong backscattering near the electron plasma frequency at densities beyond the quarter critical. This novel instability, recognized in recent experiments as stimulated laser scattering on a trapped electron-acoustic mode (SEAS), is absent from a classical theory of laser-parametric instabilities. A parametric excitation of SEAS instability, is explained by a three-wave resonant decay of the incident laser light into a standing backscattered wave and a slow trapped electron-acoustic wave ($\omega < \omega_p$). Large SEAS pulsations, eventually suppressed by relativistic heating of electrons, are observed in our simulations. This phenomenon seems relevant to future hohlraum target and fast ignition experiments.

1 Introduction

A general issue in laser fusion that has been of considerable interest in past decades is growth of instabilities in underdense plasmas [1]. Stimulated Raman and stimulated Brillouin scattering (SRS and SBS, respectively) are known as major processes that can bring high reflectivity and undesirable target preheat to prevent efficient compression of the fuel. Although much effort has been devoted to this subject [2-5], observations and theoretical models are rarely in good agreement. Recently, there are extensive activities to study plasmas at conditions appropriate to the National Ignition Facility (NIF) [6-8]. In particular, design on high temperature hohlraums (HTH) for NIF is currently underway [9]. In these HTH targets with large, moderate density plasmas, strong SRS backscatter and beam filamentation are expected at higher laser intensities.

More recently, a new type of stimulated scattering on the so-called, electron-acoustic wave (EAW) was proposed by Montgomery et al. [10, 11] to reinterpret underdense plasma data from the Trident laser facility. It was shown, that among electronic instabilities, stimulated scattering of laser light from a trapped electron-acoustic wave (SEAS) ($\omega < \omega_p$) can possibly explain anomalous backscatter data at $I > 10^{16}$ W/cm^2 previously attributed to stimulated Raman back-scattering (B-SRS) from unrealistically low plasma density. In Maxwellian plasmas, a slow linear electron-acoustic mode is strongly Landau-damped; however, at large EAW amplitudes, electron trapping can support undamped travelling modes (BGK-alike) [12] or with a small dissipation, weakly damped travelling solutions [13]. In the experiments reported, the SEAS to SRS signal ratio was smaller than 10^{-3}. However we find plasma conditions such that SEAS can dominate over B-SRS. We model SEAS and explain its onset as a 3-wave absolute instability and discuss related strong electron heating and relativistic laser-intensity regimes.

2 Simulations

To investigate stimulated laser scattering in an underdense plasma, one-dimensional particle-in-cell simulations were performed with an open-boundary electromagnetic relativistic code [14-15]. A plasma layer was placed in vacuum with more than 50 electrons/cell, while ions were kept immobile to create a neutralizing background. For energetic electrons and electromagnetic waves that reach system boundaries, two extra damping regions at the system ends were introduced (see Fig.3 of Ref. [15]). A laser with an intensity $\beta = eE_0/(mc\omega_0) = 0.6$ (E_0 is the electric field) interacts with an initially uniform plasma layer of length $L = 50c/\omega_0$ (ω_0 is the laser frequency) with the electron temperature $T = 500$eV and plasma density (a) $n = 0.1n_{cr}$, (b) $n = 0.25n_{cr}$, (c) $n = 0.5n_{cr}$ and (d) $n = 0.8n_{cr}$ ($n_{cr} = n(\omega_0/\omega_p)^2$ is the critical density; $\omega_p = (ne^2/(\varepsilon_0 m\gamma))^{1/2}$ is the electron plasma frequency and γ is the relativistic factor). To illustrate the plasma response to a step-function, linearly-polarized laser pulse, in Fig. 1, the time evolution of the reflectivity is plotted. ($R = \langle S_r \rangle/\langle S_0 \rangle$, S_r and S_i are Poynting vectors for reflected and incident wave, respectively, and $\langle\ \rangle$ denotes time averaging over the laser period). As seen in Fig. 1, the reflectivity of the plasma layer, increases with density increase, due to growing plasma instabilities. It is known that SRS, the scattering of laser light from electrostatic Langmuir waves $\omega_{EPW}^2 = \omega_p^2 + 3v_t^2 k_{EPW}^2$ (here ω_{EPW} and k_{EPW} are the electron plasma-Langmuir wave frequency and wavenumber, respectively, $v_t = (T/m)^{1/2}$ is the electron thermal velocity), plays a major role in low-density regions ($n \leq 0.25n_{cr}$) of a plasma. Since, due to relativistic electron-mass variation, the effective electron plasma frequency decreases at high laser intensities, matching conditions for B-SRS instability $\omega_0 = \omega_s + \omega_{EPW}$ and $\mathbf{k_0} = \mathbf{k_s} + \mathbf{k}_{EPW}$ can shift to higher density plasma regions beyond the $n_{cr}/4$ (here k_0 is the laser wavenumber and ω_s and k_s are the frequency and the wavenumber of the scattered light, re-

spectively). However, in the weakly-relativistic case ($\beta = 0.6$, laser intensity $I \sim 10^{17}\mathrm{W/cm^2}$), considered above, the relativistic shift is not large enough to explain high reflectivities in Figs. 1c-1d, as directly related to stimulated Raman backscattering by Langmuir waves. To obtain further insight into underdense laser-plasma instabilities, simulation data for two connected plasma layers L_1 and L_2 are shown in Fig. 2. The uniform plasma densities are $n_1 = 0.15n_{cr}$ and $n_2 = 0.5n_{cr}$ and lengths $L_1 = 30c/\omega_0$ and $L_2 = 60c/\omega_0$, respectively, with the laser strength $\beta = 0.3$ and the same initial electron temperature $T = 500\mathrm{eV}$. In fact, in Fig. 2 we show the electron phase space (longitudinal velocity versus position) at different moments of time, $t\omega_0 = 85$ and $t\omega_0 = 1380$. Our choice of densities is such that layer L_1 allows strong Raman backscattering ($n < 0.25n_{cr}$), while L_2 density is overcritical to excite SRS and serves as a heat sink. As a product of B-SRS in L_1, a large trapped Langmuir wave and forward acceleration of hot electrons from L_1 into L_2 are seen in Fig. 2, for $t\omega_0 = 85$. As expected, during this early phase, no instability in the layer L_2 is observed. However, at later times ($t\omega_0 = 1380$) "non-activity" of the heated L_2 is broken by the growth of a huge trapped EAW which strongly reflects laser light (SEAS) and further heats the system. Since this instability takes place in long higher density regions, in general, reflectivity can become large, beyond the SRS level (see also Fig. 1c and 1d, for transient peaks with more than 100% instantaneous reflection). Intermittent pulsations and instant reflectivities larger than 1, already found in B-SRS simulations, are generic to the 3-wave resonance detuning by nonlinear frequency shifts due to electron/ion trapping, relativistic effects, etc. [5,15].

3 SEAS model

Let us try to briefly explain the growth of the observed strong backscatter within a density range $n > 0.25n_{cr}$. Such a process has been recently reported by these authors [14],

recognized as SEAS instability. Through extensive particle simulations it has been found that SEAS is the parametric decay of the laser light into a backscattered light (Stokes mode) and a large electrostatic electron-acoustic wave (EAW(ω_a, k_a)). Furthermore, the main characteristic of this decay is that the backscattered wave is driven near critical, i.e. $\omega_s \approx \omega_p$ which implies $k_s \approx 0$ and $V_s \approx 0$ ($V_s \approx 0$ is the group velocity of the scattered wave). Therefore, the backscattered wave is a slowly propagating (standing) EM wave such that the frequency and wave number of EAW match a 3-wave resonance, as $\omega_a = \omega_0 - \omega_s \approx \omega_0 - \omega_p$ and $k_a = k_0 - k_s \approx k_0$. Indeed, in an early SEAS phase, observed narrow spectrum readily obeys the above frequency matching (see Fig.1 of ref. [14]). It seems apparent from above results that the EAW growth in plasmas with $n > 0.25n_{cr}$ occurs over the frequency range (well) below the electron plasma frequency ($\omega_a = \omega_0 - \omega_p$). In order to clarify the growth of such ES waves we discuss a simple model for parametric coupling between three waves, $a_i(x, t)\exp[i(k_i x - \omega_i t)]$, satisfying the frequency and wave-vector resonant matching conditions, which for weakly varying envelopes [17, 18] in dimensionless units [15], reads

$$\frac{\partial a_0}{\partial t} + V_0\frac{\partial a_0}{\partial x} = -M_0 a_s a_a, \qquad (1)$$

$$\frac{\partial a_s}{\partial t} - V_s\frac{\partial a_s}{\partial x} = M_s a_0^* a_a, \qquad (2)$$

$$\frac{\partial a_a}{\partial t} + V_a\frac{\partial a_a}{\partial x} + \Gamma_a a_a = M_a a_0^* a_s. \qquad (3)$$

where $V_i > 0$ are group velocities, Γ_a is a damping rate for EAW ($\Gamma_0 = \Gamma_s = 0$ for EM waves is used), $M_i > 0$ are the coupling coefficients and a_i are the wave amplitudes, where $i = 0, s, a$, denote the pump, backscattered wave and EAW, respectively. With standard (open) boundary conditions, $a_0(0, t) = E_0$, $a_s(L, t) = a_a(0, t) = 0$, the backscattering grows as an absolute instability, only if

$$L/L_0 > \pi/2, \qquad (4)$$

where $L_0 = (V_s V_a)^{1/2}/\gamma_0$ is the interaction length and $\gamma_0 = E_0(M_s M_a)^{1/2}$ is the uniform

growth rate [17, 18]. Since for the backscatter we have typically observed $V_s \approx 0$, the condition (4) is readily satisfied ($L_0 \approx 0$), even for a weak growth rate. An explicit form of the left hand side of (1) and (2) is easy to get (light waves). Although for EAW no linear dispersion relation in analytical form exists [14], the real part of the frequency is derived to scale like $\omega_a \approx \alpha k_a v_t$, where various authors find $\alpha \approx (1-3)$ [12,13,16]. Due to a nonzero damping $\Gamma_a \neq 0$, EAW is characterized by the longitudinal absorption length $L_a = V_a/\Gamma_a$, so SEAS-backscatter becomes absolute under an extra condition [18],

$$L_0/L_a < 2. \tag{5}$$

In a linear theory EAW is a highly damped slow ES mode, so that the absorption length L_a takes small values. Still, the key factor for onset and growth of SAES is a nearly critical "standing" backward Stokes wave ($L_0 \approx 0$), such that $V_s \approx 0$ satisfies (5) and also minimizes the threshold for SEAS excitation [18], according to $\gamma_0 > 0.5\Gamma_a(V_s/V_a)^{1/2}$.

4 Discussions

In Figure 3 we display the electromagnetic (EM) and electrostatic (ES) spectrum for parameters of Fig. 1d corresponding to a developed SEAS stage ($t\omega_0 = 110 - 842$). The incident laser light ($\omega_0 = 1$) decays into a spectrally broadened backscattered light and a slow trapped EAW, centered around ($\omega_s \approx 0.72$) and ($\omega_a/\omega_0 \approx 0.28 << \omega_{p0}/\omega_0 \approx 0.89$), respectively. This figure confirms the basic SEAS scheme. The effective electron plasma frequency ω_p is much smaller than its standard non-relativistic value ω_{p0}, basically due to an increasing relativistic γ - factor (vide supra). A dynamical locally reduced ω_p can effectively trap a slowly propagating EM Stokes wave inside the plasma. Moreover, instead of narrow spectra at an early stage [14], the SEAS broadened incoherent spectra are observed at late times in Fig. 3. At large amplitudes, trapping and relativistic nonlinearities induce resonance

broadening and strong electron heating which result in a complex SEAS saturation [5,15]. The above picture seems to be generally consistent with the 3-wave backscatter complexity model, proposed by one of these authors [15].

To illustrate the spatial variation of EM and ES fields in the plasma layer ($n = 0.6n_{cr}$, $L = 40c/\omega_0$, $\beta = 0.3$), snapshots for a weak pumping case are shown in Fig. 4a. According to [13] efficient resonant EAW excitation is expected for $\omega_a/k_a v_t = 1-2$, which for above parameters would require $v_t/c \approx 0.28$. Although somewhat unrealistic, such high longitudinal electron temperatures can be produced due to forward and backward SRS. As a weak pump ($\beta = 0.3$) appears to be close to an instability threshold (for parameters in Fig. 4) we find SEAS sensitive to exact temperature matching: no instability was observed outside the range $v_t/c = (0.18 - 0.30)$ [14]. This is contrary to a stronger pump case (e.g., $\beta = 0.6$) where relativistic resonance broadening seems to enable SEAS growth (vide supra, Fig. 1) at much lower temperatures [14]. An early response ($t\omega_0 = 1936$) is nearly a steady-state, with a nonlinearly (ponderomotively) driven ES waves at the second ($2\omega_0, 2k_0$) and at the zero (0,0) harmonics [16]. The fully developed SEAS instability is visible in Fig. 4a for $t\omega_0 = 2969$, characterized by large amplitude EM and ES waves. After plasma relaxes by an instability propagating out in the backward direction ($t\omega_0 = 3098$), new growth takes place (see Fig. 4a for $t\omega_0 = 3227$). Above features appear well correlated with the corresponding reflectivity pulsations observed in Fig. 4b. We note that after the first growth and relaxation, the system is already significantly heated which results in a shift in the matching condition and eventual suppression of further growth. Finally, let us discuss possible consequences of stimulated scattering instabilities excited in an underdense plasma toward the high density core. In Fig. 5, the reflectivity and transmittivity for the system consisting of two connected plasma layers L_1 and L_2 (the densities are $n_1 = 0.2n_{cr}$ and $n_2 = 0.6n_{cr}$, the lengths are $L_1 = 20c/\omega_0$ and

$L_2 = 80c/\omega_0$, the laser strength is $\beta = 0.3$ and the temperature is $T = 500\text{eV}$) is plotted. The first phase $t\omega_0 < 2400$ corresponds to a decreasing efficiency of laser penetration through a plasma, due to strong SRS reflection in L_1. After B-SRS instability gets fully developed (in Fig. 5 for $t\omega_0 \approx 500$), transmittivity gradually increases following B-SRS supression due to a generation of hot electrons. The second large drop in transmittivity (see Fig. 5 for $t\omega_0 \approx 2500$) is attributed to an intense SEAS reflection from layer L_2 which was heated up by hot electrons transported from L_1. As observed, fast SEAS growth produces a rapid cut-off in the laser propagation. This is important, since such a phenomenon can possibly interrupt a delivery of a laser beam energy to the hohlraum. Furthermore, a complex and intermittent SEAS dynamics can result in a large variation in laser intensity at a critical surface of the target. Another aspect is related to huge plasma heating, illustrated in Fig. 6 in which longitudinal electron distributions for parameters of Fig. 1d are shown. SEAS instability strongly deforms the initial Maxwellian ($t\omega_0 = 0$) into a relativistic "water-bag like" distribution ($t\omega_0 = 1120$). Further instability growth additionally heats up the plasma until SEAS gets fully suppressed ($t\omega_0 = 2500$).

5 Conclusions

Although there has been a significant effort to understand a complicated picture of underdense plasma instabilities and their impact on the NIF target plasmas, in most cases, obtained results, including those presented in this paper, show a variety of phenomena that can lead to an unexpectedly large and anomalous plasma response. It was shown, that, apart from B-SRS, a significant reflection and the plasma core preheat can be due to a novel SEAS; in particular, in underdense plasma regions beyond $n_c/4$. The possibility of exciting such intense ES waves in large IFE targets deserves future attention. In particular, we plan to further address a relative role and synergy between SEAS and SRS by more realistic simulations in nonuniform plasmas.

References

[1] W. L. Kruer, Interaction of plasmas with intense lasers, Phys. Plasmas 7, 2270 (2000).

[2] H. A. Rose, Langmuir wave turbulence transition in a model of stimulated Raman scatter, Phys. Plasmas 7, 2571 (2000).

[3] R. L. Berger et al., On the dominant and subdominant behavior of stimulated Raman and Brillouin scattering driven by nonuniform laser beams, Phys. Plasmas 5, 4337 (1998).

[4] W. L. Kruer et al., Interplay between laser plasma instabilities, Phys. Scripta T 75, 7 (1998).

[5] H. X. Vu et al., Kinetic inflation of stimulated Raman backscatter in regimes of high linear Landau damping, Phys. Plasmas 9, 1745 (2002).

[6] D. S. Montgomery et al., Evidence of plasma fluctuations and their effect on the growth of stimulated Brillouin and stimulated Raman scattering in laser plasmas, Phys. Plasmas 5, 1973 (1998).

[7] J. C. Fernández et al., Observed intensity of stimulated Raman scattering on electron density, Phys. Plasmas 7, 3743 (2000).

[8] H. X. Vu et al., Transient enhancement and detuning of laser-plasma parametric instabilities by particle trapping, Phys. Rev. Lett. 86, 4306 (2001).

[9] D. E. Hinkel et al., *Laser-plasma interactions in high temperature hohlraums*, in Inertial Fusion Science and Applications 2001, eds. K.A. Tanaka et al. (Elsevier, Paris, 2002), p. 291.

[10] D. S. Montgomery et al., *Observation of stimulated electron-acoustic-wave scattering*, Phys. Rev. Lett. **87** (2001);

[11] D. S. Montgomery et al., *Recent Trident single hot spot experiments: Evidence for kinetic effects, and observation of Langmuir decay instability cascade*, Phys. Plasmas **9**, 2311 (2002).

[12] J. P. Holloway and J. J. Dorning, *Undamped plasma waves*, Phys. Rev. A **44**, 3856 (1991).

[13] H. A. Rose and D. A. Russell, *A self-consistent trapping model of driven electron plasma waves and limits on stimulated Raman scatter*, Phys. Plasmas **8**, 4784 (2001).

[14] Lj. Nikolić et al., *Stimulated electron-acoustic-wave scattering in a laser plasma*, Phys. Rev. E **66**, 036404 (2002).

[15] S. Miyamoto et al., *Simulations of anomalous stimulated Raman backscattering in a bounded plasma*, J. Phys. Soc. Jpn. **67**, 1281 (1998); M.M. Škorić et al., *Transition to turbulence via spatiotemporal intermittency in stimulated Raman backscattering*, Phys. Rev. E **53**, 4056 (1996).

[16] F. W. Sluijter and D. Montgomery, *Secular and nonsecular behavior for the cold plasma equations*, Phys. Fluids **8**, 551 (1965).

[17] R. W. Harvey and G. Schmidt, *Three wave backscatter interactions in a finite region*, Phys. Fluids **18**, 1395 (1975).

[18] D. W. Forslund et al., *Theory of stimulated scattering processes in a laser-irradiated plasmas*, Phys. Fluids **18**, 1002 (1975).

Figure Captions

Fig. 1. Reflectivity in time for plasma layers (a) $n = 0.1n_{cr}$, (b) $n = 0.25n_{cr}$, (c) $n = 0.5n_{cr}$ and (d) $n = 0.8n_{cr}$ ($L = 50c/\omega_0$, $T = 500\text{eV}$, $\beta = 0.6$).

Fig. 2. Electron velocity versus position for two connected plasma layers ($n_1 = 0.15n_{cr}$, $L_1 = 30c/\omega_0$, $n_2 = 0.5n_{cr}$, $L_2 = 60c/\omega_0$, $\beta = 0.3$, $T = 500\text{eV}$) for $t\omega_0 = 85$ and $t\omega_0 = 1380$ showing large trapping orbits. The laser pulse is injected into L_1 with an interface between two layers at $X = 30c/\omega_0$.

Fig. 3. Spectrum of electromagnetic (top) and electrostatic (bottom) waves in the plasma layer ($n = 0.8n_{cr}$, $L = 50c/\omega_0$, $T = 500\text{eV}$, $\beta = 0.6$) for a time interval $t\omega_0 = 110 - 842$.

Fig. 4. (a) Snapshots of the spatial evolution of electromagnetic (EM) and electrostatic (ES) fields in the plasma layer ($n = 0.6n_{cr}$, $L = 40c/\omega_0$) for initially high electron temperature $v_t/c = 0.28$ and a weak pump $\beta = 0.3$; versus (b) the corresponding Reflectivity in time.

Fig. 5. Reflectivity (top) and Transmittivity (bottom) in time for two connected plasma layers ($n_1 = 0.2n_{cr}$, $L_1 = 20c/\omega_0$, $n_2 = 0.6n_{cr}$, $L_2 = 80c/\omega_0$, $\beta = 0.3$, $T = 500\text{eV}$).

Fig. 6. Electron velocity distribution in time ($n = 0.8n_{cr}$, $L = 50c/\omega_0$, $T = 500\text{eV}$, $\beta = 0.6$) for $t\omega_0 = 0$, $t\omega_0 = 1120$ and $t\omega_0 = 2500$.

(a)

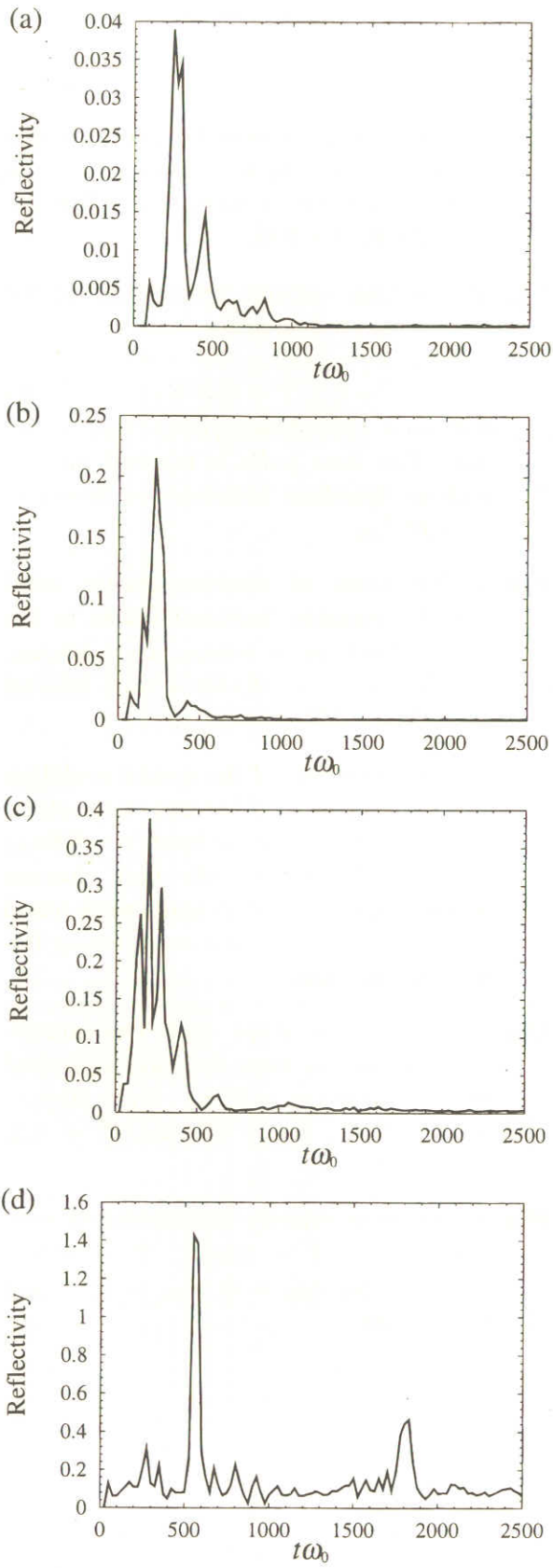(b)

(c)
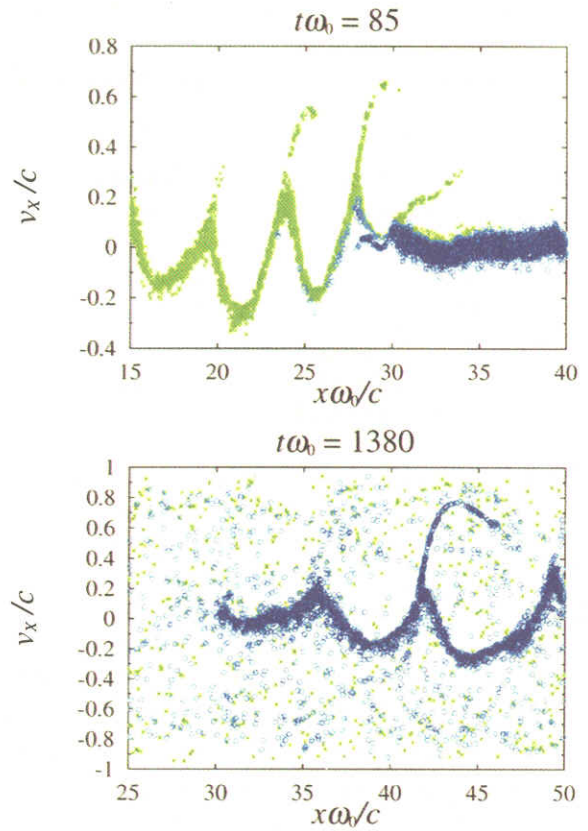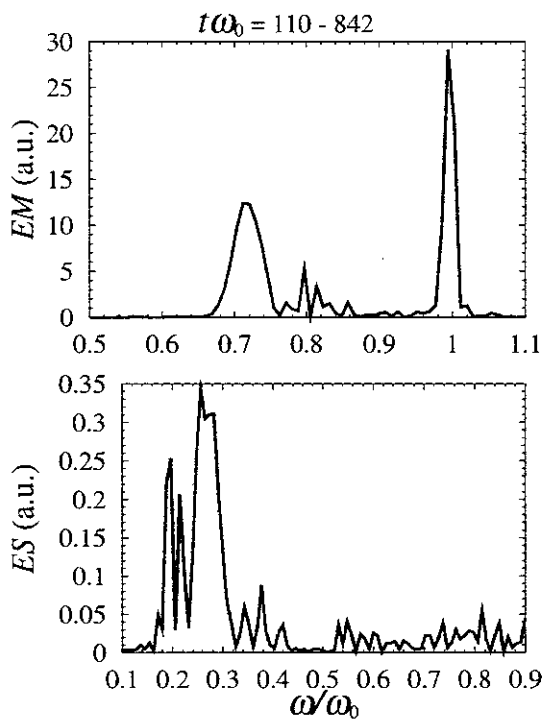
(d)

$t\omega_0 = 85$

$t\omega_0 = 1380$

Fig. 2

Fig. 1

$t\omega_0 = 1936$

Electric field

$x\omega_0/c$

ES ——
EM ------

$t\omega_0 = 110 - 842$

EM (a.u.)

ES (a.u.)

ω/ω_0

Fig. 3

$t\omega_0 = 2969$

Electric field

$x\omega_0/c$

ES ——
EM ------

$t\omega_0 = 3098$

Electric field

$x\omega_0/c$

ES ——
EM ——

$t\omega_0 = 3227$

Electric field

$x\omega_0/c$

ES ——
EM ------

Fig. 4a

Fig. 4b

Fig. 6

Fig. 5